



Green synthesis of novel silver nanocomposite hydrogel based on sodium alginate as an efficient biosorbent for the dye wastewater treatment: prediction of isotherm and kinetic parameters

G. Karthiga Devi, P. Senthil Kumar*, K. Sathish Kumar*

Department of Chemical Engineering, SSN College of Engineering, Chennai 603 110, India, Tel. +91 9626555678; email: devigk19@gmail.com (G. Karthiga Devi), Tel. +91 9884823425; email: senthilchem8582@gmail.com (P. Senthil Kumar), Tel. +91 9962570234; email: sathishkumark@ssn.edu.in (K. Sathish Kumar)

Received 5 January 2016; Accepted 8 April 2016

ABSTRACT

This paper is focused on simple, cost-effective and one-step green synthesis of silver nanocomposite hydrogel (SNC) based on sodium alginate toward the removal of methylene blue (MB) dye from aqueous solutions. *Mukia maderaspatna* plant extract was used as a reducing agent and the reaction occurred at room temperature. The novel SNC was characterized by Fourier transform infrared spectroscopy (FTIR), scanning electronic microscope (SEM), transmission electron microscope (TEM), thermogravimetric analysis (TGA), and X-ray diffraction (XRD) analyses. The FTIR results observed indicated the presence of silver ions in the inside of the hydrogel composite. The XRD results revealed that the SNC are crystalline in nature. It was observed from the TEM results that the particle size of Ag nanoparticles was around 19 nm. Furthermore, the prepared SNC was found to exhibit excellent adsorbent properties for the removal of MB dye from the aqueous solution. This has been experimentally studied through Langmuir, Freundlich, Redlich–Peterson, and Sips adsorption isotherms. The maximum Langmuir monolayer adsorption capacity was calculated as 213.7 mg of MB dye/g of SNC. The pseudo-first-order, pseudo-second-order, and Elovich kinetic models were used to fit the adsorption kinetics data. The prepared SNC can be effectively utilized for the removal of dyes from the industrial wastewater.

Keywords: Plant extract; Silver nanocomposite; Adsorption; Kinetics; Isotherms

1. Introduction

Since the end of the last century, a variety of wastes from chemical and pharmaceutical industries have been released into the environment through wastewater streams. These effluents mainly consist of surfactants, disinfectants, detergents, and personal care products. One of the major forms of pollutants is dye

wastes and has become a major environmental threat drawing concerns globally. Currently, most of the dye wastes are being treated using physical and chemical treatment methods [1,2] but they fail to remove dyes completely considering that they are not degradable in nature [3]. Therefore, it is necessary to take sustainable initiatives that use principles from green chemistry to remove the dyes before releasing into the aquatic system. For ages, catalysis has been one of the most common techniques used for the degradation of

*Corresponding authors.

organic dyes into nontoxic substances in wastewater [4,5]. Although this process requires a shorter period of time for degradation, it requires toxic chemicals for reduction to occur. At the moment, many novel treatment methods such as biodegradation [6], adsorption [7], advanced oxidation [8], nanofiltration [9], and photocatalysis [10] are being employed for the treatment of dyes. Adsorption has been found to be promising among all other techniques due to its simple design and operation [11]. Many natural materials from agricultural operations [12] as well as industrial wastes [13] have been evaluated as potential adsorbents for the removal of dyes from wastewater. But the production of secondary byproducts after the treatment limits their applications. Therefore, scientists have been exploring the new technologies in the production of new types of adsorbent materials.

Progress in the field of nanotechnology has created an emerging trend in wastewater treatment with its improved possibility of innovative products and processes [14]. Generally, nanomaterials are classified into 4 groups which are particularly considered important materials in water treatment namely; dendrimers, metal-containing nanoparticles, zeolites, and carbonaceous nanomaterials. The ability of metal nanoparticles to be tailored into different morphologies has motivated an upsurge for it in various applications [15]. Because of the smaller size, large surface area and the fact that it can be easily anchored to polymer matrices, it exhibits efficient removal of dye molecules [16]. In particular, silver nanoparticles occupy prime attention in the treatment of organic pollutants from wastewater under ambient conditions [17]. Previously, graphene oxide-based silver nanoparticles containing composite hydrogels have been acting as a promising material for removal of organic dye pollutants from an aqueous environment [18]. Titanium dioxide nanoparticles immobilized in calcium alginate has also been used for the removal of textile dyes [19] and the TiO_2 immobilized on chitosan-based hydrogels for the degradation of azo dyes [20].

In the recent years, attempts have been made to synthesize silver nanoparticles from natural agents [21,22], plants have received an increasing attention for the synthesis of metal nanoparticles [23]. The researcher's attention has been focused on incorporating these metal nanoparticles onto the polymer support because the physicochemical features of the polymer support with the chemical properties of the polymer-bound functional groups and the catalytic efficiency of the supported metal nanoparticles offer possibilities for the generation of innovative catalyst [24]. On the basis of previous works [25], it is proposed here that a simple and one-step procedure

for preparing size-controlled silver nanoparticle using *Mukia maderaspatna* aqueous leaf extract. This plant has been chosen due to its excellent reducing property. Biologically synthesized silver nanoparticles incorporated with biodegradable sodium alginate grafted-polyacrylic acid lead to the formation of poly-ionic hydrogel microbeads. The synthesis of hydrogel microspheres occurs through ionotropic gelation methods which are found to be simple and time-consuming. The incorporation of metal nanoparticles into the porous structures improves the physical and chemical nature of the nanocomposite hydrogel toward a variety of applications [26]. There are some reports about the impact of carbopol polymers on attributes of calcium-alginate beads [27–29] but none for Carbopol 937 in the context of dye degradation applications.

MB dye is one of the major pollutants released from many industries which results in serious health problems to human as well as aquatic systems. These dyes are difficult to remove from the environment using conventional treatment methods because of the presence of aromatic amines in their structures as they are non-degradable in nature. Therefore, it is necessary to find an alternative cost-effective method for the removal of the dyes from the wastewater before discharge. The objective of the present research is to investigate the adsorption potential of green synthesized silver nanocomposite (SNC) toward the removal of methylene blue (MB) dye from the wastewater. The adsorption equilibrium data were analyzed using the Langmuir, Freundlich, Redlich–Peterson, and Sips isotherm equations. The adsorption kinetic data were tested with the pseudo-first-order, pseudo-second-order, and Elovich kinetic models.

2. Materials and methods

2.1. Materials

The natural polysaccharide sodium alginate was obtained from Sigma–Aldrich Chemicals, Chennai and used as procured. The polymer Carbopol 937, the redox initiator potassium persulfate, and the crosslinker calcium chloride were obtained from Himedia Chemicals, Chennai. Silver nitrate and the synthetic organic MB dye (molecular weight 319) were purchased from S.D. Fine Chemicals, Mumbai. These chemicals were of analytical grades and used without purification.

2.2. Methods

2.2.1. Preparation of plant extract

M. maderaspatana leaves were purchased from local markets. The plants were authenticated and voucher

specimen has been deposited as HPRKVK 2013-097 in the herbarium of Botany department, Presidency College, Chennai, India, for plant identification. About 3 g of *M. maderaspatana* was washed using deionized water several times and then boiled with 150 ml of deionized water for 5 min. The extract was filtered and used for further experiments.

2.2.2. Biosynthesis of silver nanoparticles

The silver nanoparticles were prepared according to a previous protocol [30]. In brief, silver nitrate (0.16 g) was dissolved in 100 ml of the deionized water and stirred for 1 h to obtain 0.01 M solution. About 5 ml of freshly prepared plant extract (2%) was then added to 95 ml silver nitrate (1 mM) solution dropwise under the constant stirring condition and incubated for 1 h in sunlight. The mixture was then allowed to cool at 4°C and the pH of the reaction medium was increased to 5.0 using 1 M NaOH solution. A colloidal brown color was formed within a few minutes, which was then centrifuged at 10,000 rpm for 30 min. The pellet obtained was washed several times with distilled water to remove the unreacted chemicals. The obtained silver nanoparticles were dried using lyophilizer.

2.2.3. Synthesis of carbopol–alginate beads (CAA)

The carbopol–alginate hydrogel beads (CAA) were prepared by ionotropic gelation technique [31]. Initially, the aqueous solution (2% w/v) of sodium alginate was prepared by gentle mixing and stirring of sodium alginate in distilled water. The reaction was carried out in three-neck glass reactor at 30°C and the reaction volume was made up to 50 ml by the addition of (0.5% w/v) Carbopol 937 solution. The initiator (0.05% w/v) was then added and the reaction was purged with nitrogen gas for a few minutes. The reactor was stirred continuously for 4 h till the mixture got gelled. The CAA hydrogel beads were prepared by dropping the suspension using syringe into a gently stirred mixture of (0.25 mM) calcium chloride and (150 mM) sodium chloride solution. The hydrogel beads were collected and washed with deionized water repeatedly to remove the residual crosslinkers and initiators. The CAA beads were dried by lyophilizer to a constant weight. The dried hydrogel beads were milled using a mortar and sieved to a particle size of 60 µm.

2.2.4. Synthesis of Ag-CAA beads (SNC)

To prepare the Ag-incorporated CAA nanocomposite hydrogels, 100 mg of the dry hydrogel beads (CAA) were taken and immersed in water for 3 d to

swell to their maximum size. About 100 mg of swollen CAA beads were transferred into 25 ml of 1 mM silver nitrate solution followed by incubation for 12 h under constant stirring condition. During this period, the incorporation of silver ions into the CAA hydrogel beads occur. The silver ion-loaded CAA hydrogel beads were wiped off with tissue paper and dispersed in 50 ml of 2% aqueous mukia leaf extract solution. The beaker was kept in the sunlight for 240 min in order to reduce the silver ions into silver nanoparticles. The Ag-incorporated hydrogel beads were washed with deionized water several times to remove unreacted silver ions and were allowed to dry at room temperature. The obtained Ag incorporated hydrogel beads are termed as SNC nanocomposite.

2.2.5. Swelling of the hydrogel beads

For analyzing the swelling phenomenon, the known weight (0.3 g) of the dried SNC was equilibrated in 100 ml of distilled water or buffer solution at room temperature. The beads were withdrawn at regular intervals of time (2 h) and wiped off with filter paper to remove the excess solution. Beads are weighed carefully without much force from pressing. The hydrogel beads were kept in the distilled water till it attains its equilibrium. The percentage of equilibrium swelling was calculated using the formula:

$$\text{Equilibrium swelling (\%)} = \left(\frac{S_w - S_i}{S_i} \right) \times 100 \quad (1)$$

where S_w is the weight of swollen beads at equilibrium and S_i is the dry weight of beads.

2.2.6. Fourier transform infrared (FTIR) spectroscopy

FTIR spectroscopy was used to study the incorporation of silver ions onto the hydrogel network. The FTIR spectra of Ag nanoparticles, CAA beads, and SNC beads were recorded on a Perkin Elmer Spectra 100 Spectrophotometer. The samples were dried in a vacuum oven prior to the spectral measurement. About 1 mg of the sample was placed on the crystal surface and the spectra were recorded from 4,000 to 400 cm^{-1} .

2.2.7. X-ray diffraction (XRD)

The nature of the SNC nanocomposite was recorded by XPERT-PRO diffractometer using Cu K α radiation ($\lambda = 1.5406 \text{ \AA}$). The scanning was performed in the region of 2θ from 20° to 90°.

2.2.8. Scanning electron microscopy–energy dispersive spectroscopy (SEM–EDAX) analysis

The colloidal nanocomposite solution was centrifuged at 10,000 rpm for 10 min, the pellets obtained were taken. It is then dissolved completely in 0.1 mL of deionized water and it was mounted onto the grid coated with gold. It was then allowed to dry and remove the excess solution using blotting paper. The morphology and elemental composition of the nanocomposite were studied using scanning electron microscope (Supra-55, Carl-Zeiss, Germany) with an accelerating voltage of 10 kV equipped with EDAX analyzer (ZEISS Gemini-300). The software is Smart-SEM and the imaging mode is inlens detector. The details regarding applied voltage, magnification used, and size of the contents of the images were implanted on the images.

2.2.9. Transmission electron microscopy

The size of the SNC beads was measured using JEOL JEM 2100 Transmission Electron Microscope (TEM). A drop of the centrifuged sample (1 mg/ml) of the dried SNC nanocomposite solution was placed on the Cu grid covered with a thin film and allowed to dry. The instrument was operated with an accelerating voltage of 100 kV.

2.2.10. Thermal gravimetric analysis (TGA) and differential scanning calorimetric (DSC) analysis

The thermal stability of the synthesized SNC nanocomposite was studied by simultaneous thermogravimetric analysis and differential scanning calorimetric measurements under a nitrogen atmosphere at a flow rate of 100 ml/min with the heating rate of 10°C per min. TGA and DSC analysis of SNC nanocomposite were carried out with Mettler Toledo TGA/SDTA System (Greifensee, Switzerland). About 2 mg of SNC nanocomposite were used for the TGA and DSC analysis. The thermograms were taken between a temperature range of (0–600°C). The graph was drawn between percentage weight loss and temperature.

2.2.11. UV–vis analysis

The formation of silver nanoparticle synthesis was confirmed using UV–vis spectroscopy analysis (JASCO V-630) scanned from 200 to 800 nm and recorded at a scanning speed of 1 nm intervals.

2.2.12. Study of dye removal by the nanocomposite

A known weight 0.1 g of SNC beads was immersed into 100 mL dye solution concentration (50 mg/L) and placed in an incubator shaker (150 rpm) at room temperature. After the predetermined contact time, the adsorption mixtures were centrifuged to separate the spent adsorbent and supernatant. The experiments were repeated till it reached equilibrium. For kinetic studies, the experiments were repeated by adding 0.1 g of SNC beads into 100 mL of the MB dye solutions (50–250 mg/L) and kept the agitation on for various time periods (20–180 min) at room temperature. The concentration of the dye solution before and after treatment with SNC beads was determined using UV–vis spectrophotometer (JASCO V-630, USA). The absorbance readings of the MB dye were measured at 660 nm. The amount of MB dye adsorbed onto SNC nanocomposite at equilibrium (q_e) was calculated according to the following equation:

$$q_e = \left(\frac{C_i - C_e}{m} \right) V \quad (2)$$

where q_e is the equilibrium adsorption capacity (mg/g), C_i is the initial concentration of MB dye in the solution (mg/L), C_e is the equilibrium concentration of MB dye in the solution (mg/L), V is the volume of the aqueous dye solution (mL), and m is the mass of SNC beads employed [32,33]. Likewise, adsorption or the percentage removal (R %) was calculated as:

$$\% R = \left(\frac{C_i - C_e}{C_i} \right) \times 100 \quad (3)$$

Here C_i and C_e are the initial and equilibrium concentration of the MB dye solution (mg/L), respectively, and V is the volume (L) of the dye solution.

2.3. Data fitting with adsorption isotherm and kinetic models

2.3.1. Adsorption isotherm studies

Adsorption isotherms provide the adsorption mechanism. This gives the relationship between the amount of dye adsorbed at equilibrium (q_e) and the concentration of the remaining dye in solution at equilibrium (C_e). Under the equilibrium condition, the adsorption efficiency obtained at 30°C against different MB dye concentrations is used to construct the four adsorption

isotherm models namely; Langmuir, Freundlich, Redlich–Peterson, and Sips models.

The Langmuir adsorption isotherm model [34] is given as follows:

$$q_e = \frac{q_m K_L C_e}{1 + K_L C_e} \quad (4)$$

where q_e is the equilibrium adsorption capacity (mg/g), q_m representing the maximum adsorption capacity (mg/g), K_L is the Langmuir constant representing the adsorption energy (L/mg), and C_e is the concentration of dye solution at equilibrium (mg/L).

The Freundlich adsorption isotherm model [35] is given as follows:

$$q_e = K_F C_e^{1/n} \quad (5)$$

where K_F is the Freundlich constant ((mg/g) (L/mg)^(1/n)) and n is a measure of the deviation from linearity of adsorption (g/L). The importance of n is as follows: $n < 1$ (chemical process); $n = 1$ (linear); $n > 1$ (physical process).

The Redlich–Peterson isotherm [36] is a combination of Langmuir–Freundlich model. It approaches the Freundlich model at high concentration and is in accord with a lower concentration limit of the Langmuir equation. The equation is given as:

$$q_e = \frac{K_{RP} C_e}{1 + \alpha_{RP} C_e^{\beta_{RP}}} \quad (6)$$

where K_{RP} is Redlich–Peterson constant (L/g), α_{RP} is Redlich–Peterson constant (L/mg)^{1/β_{RP}}, and β_{RP} is the Redlich–Peterson exponent (lies between 0 and 1). The significance of β is given as follows: $\beta = 1$ (approaches Langmuir model); $\beta = 0$ (approaches Freundlich model).

Sips model [37] is given as follows:

$$q_e = \frac{K_S C_e^{\beta_S}}{1 + \alpha_S C_e^{1/\beta_S}} \quad (7)$$

where K_S is the Sips isotherm constant (L/g)^{β_S}, α_S is the Sips isotherm constant (L/g)^{1/β_S} and β_S are the Sips isotherm model exponent. The β_S is measured as the heterogeneity factor. The importance of β_S is as follows: $\beta_S > 1$ (heterogeneous process); $\beta_S = 1$ (a material with relatively homogenous binding sites). For $\beta_S = 1$, the Sips model reduces to the Langmuir isotherm

model. Adsorption equilibrium data were fitted with the above-mentioned adsorption models using MATLAB R2009 software to estimate the adsorption isotherm parameters, the coefficient of determination (R^2) and error (sum of squared errors (SSE), and root mean squared error (RMSE)) values.

2.3.2. Adsorption kinetic studies

To study the adsorption kinetics for the removal of MB dye from aqueous solution using SNC nanocomposite, the pseudo-first-order, pseudo-second-order, and Elovich kinetic models were used. The pseudo-first-order kinetic model suggested by Lagergren [38] for adsorption is given as follows:

$$q_t = q_e(1 - \exp(-k_1 t)) \quad (8)$$

where q_t is the adsorption capacity at the time (mg/g), q_e is calculated equilibrium adsorption capacity (mg/g), k_1 is the pseudo-first-order rate constant (min⁻¹), and t is the time (min).

Pseudo-second-order kinetic model [39] is given as follows:

$$q_t = \frac{q_e^2 k_2 t}{1 + q_e k_2 t} \quad (9)$$

where q_t is the adsorption capacity at the time (mg/g), q_e is calculated equilibrium adsorption capacity (mg/g), and k_2 is the pseudo-second-order rate constant (g/mg min).

Elovich kinetic model [40] is given as follows:

$$q_t = (1 + \beta_E) \ln(1 + \alpha_E \beta_E t) \quad (10)$$

where α_E is the initial adsorption rate in mg/(g min) and β_E (g/mg) is the desorption constant related to the extent of the surface coverage and activation energy for chemisorption. Adsorption kinetic data were applied to the discussed kinetic models using MATLAB R2009, the software used to estimate the adsorption kinetic parameters, R^2 , and error (SSE and RMSE) values.

3. Results and discussion

3.1. Synthesis of silver nanocomposites

Silver nanoparticles possess efficient catalytic activity and selectivity due to large surface area, size, and shape [41]. The biosynthesis procedures open new

ideas for the design of size-controlled silver nanoparticles [42]. Silver nanoparticles were synthesized by biogenic reduction of silver ions using *M. maderaspatna* extract. The UV–vis spectrophotometric analysis was used to analyze the formation of silver nanoparticles. This confirmed the formation of the absorbance band at 443 nm (Fig. 1(a)), which usually silver nanoparticles show at 350–460 nm [43]. The intensity of absorbance band increased with the increase in time up to 10 min for the complete reduction. The synthesis done by heating the reaction mixture using a magnetic stirrer was found to be time-consuming resulting in larger nanoparticles with broader size distribution.

The hydrogel beads are formed by ionic gelation of sodium alginate with carbopol 937 in the presence of initiators and crosslinker. The polymer mixture contains polyelectrolyte dropping into the counter ions present in the crosslinker solution results in the formation of beads as shown in (Fig. 1(b)). Further, the green synthesized silver nanoparticles were incorporated into the hydrogel beads with the aim to study the dye adsorption properties. Due to the inefficiency of simple mixing of hydrogel mixtures and polymerization in the presence of pre-synthesized silver nanoparticles, the incorporation was attempted using *in situ* reduction technique. This involves the dispersion of silver nanoparticles attached in the polymer matrices and the impregnation of silver ions with alginate chains followed by reduction with plant extract. This occurs based on the Van der Waals forces between the negatively charged hydroxyl and acetyl groups present on the surface of the alginate with the positive charge ions on the surface of silver nanoparticles. This method possesses some advantages over the previous extrusion/precipitation methods because the CAA template allows better dispersion of silver nanoparticles in the polymer matrix and also prevents the formation of aggregates. This template-based synthesis also leads to the formation of silver

nanocomposite (SNC) with a uniform distribution (Fig. 1(c)).

3.2. Swelling study

3.2.1. Effect of sodium alginate concentration on hydrogel swelling

The effect of sodium alginate concentration on the swelling ratio of carbopol/alginate hydrogel (CAA) is shown in Fig. 2(a). The maximum swelling was observed when the concentration of sodium alginate increases from 0.1% (w/v) to 2% (w/v) and decreased when the concentration increased above 5%. The carbopol concentration should be decreased with increase in the concentration of sodium alginate in order to avoid the increase in the density of hydrogel. The increase in molecular weight of the grafted polymer leads to the reduction in water absorbency of the hydrogel. When compared with previous studies [44], it is found that the high swelling was mainly due to the hydrophilic groups present in the sodium alginate.

3.2.2. Effect of AgNO_3 concentration on hydrogel swelling

The effect of silver nitrate concentration on hydrogel swelling capacity of the SNC nanocomposite is shown in Fig. 2(b). SNC nanocomposite was prepared with different concentrations of silver nitrate (0.001–0.005 M/L) by keeping the sodium alginate concentration at 2%. The water absorbency increases because the silver nanoparticles penetrate into the hydrogel which in turn increases the surface area. After that, the swelling capacity of the hydrogel decreases when the concentration rises above 0.005 M/L. This is mainly due to the chelation of hydroxyl and carboxyl groups of hydrogel networks by the silver ions so that water absorbency

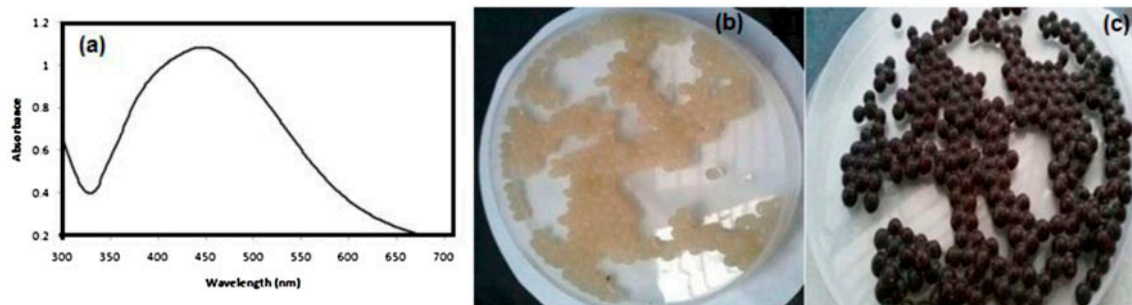


Fig. 1. (a) UV–vis spectra of silver nanoparticle formation at 443 nm, (b) hydrogel beads synthesized using carbopol 937 and sodium alginate, and (c) silver nanoparticle-incorporated hydrogel beads-SNC.

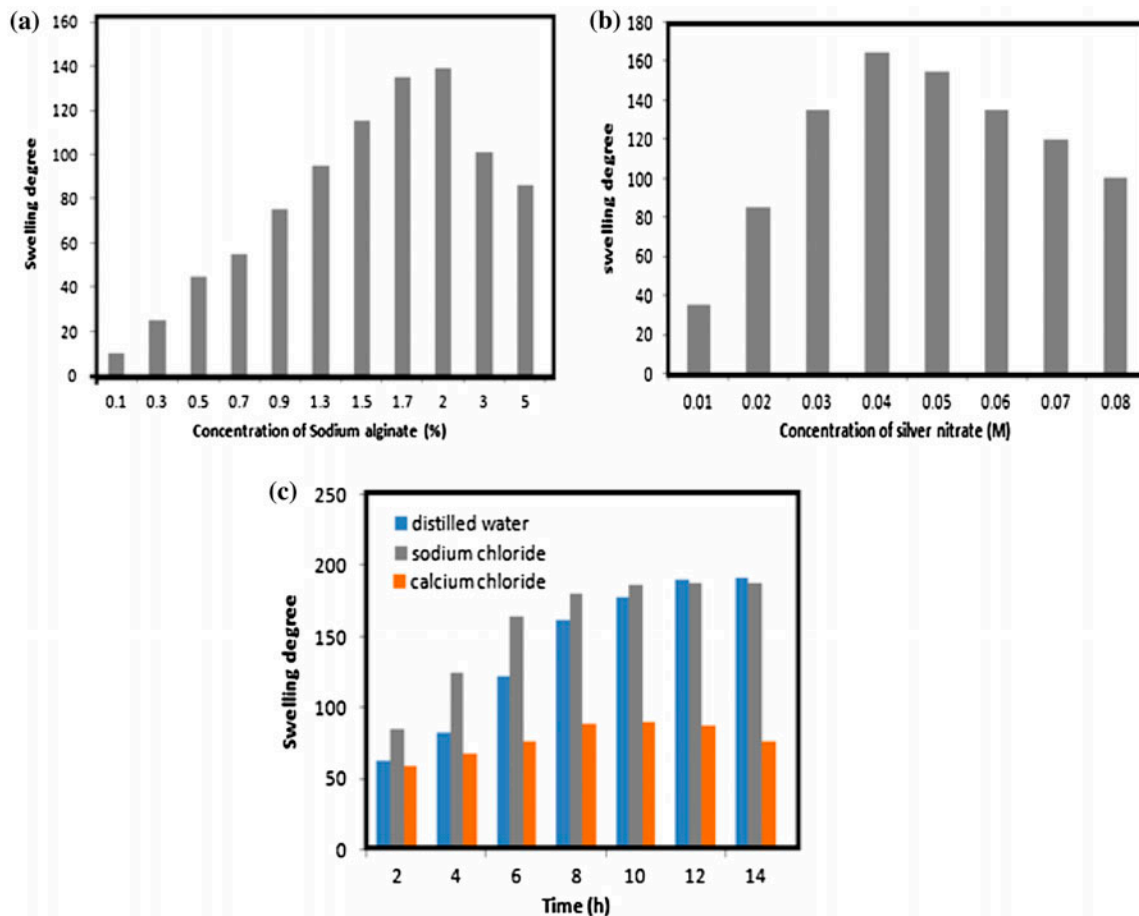


Fig. 2. (a) Effect of sodium alginate concentration on hydrogel swelling, (b) effect of AgNO₃ concentration on hydrogel swelling, and (c) effect of saline solutions on hydrogel swelling.

decreases. In this work, the SNC nanocomposite with 2% sodium alginate and 0.005 M/L of silver nitrate was chosen as an optimum concentration for further investigations.

3.2.3. Effect of saline solutions on hydrogel swelling

The swelling capacity in different saline solutions can be studied based on the swelling nature of the hydrogel with respect to the respective swelling time. The swelling capacities of SNC nanocomposite in 1 mM/L sodium chloride and calcium chloride solution are shown in Fig. 2(c). In NaCl solution, the swelling increased with the increase in time and it reached equilibrium within 8 h. Further increase in time, showed no change in swelling of the nanocomposite. In CaCl₂ solution, the water absorbency was found to be less due to the complex interactions between the carboxyl groups present in the nanocomposite with the calcium ions in the swelling medium. This creates

complex cross-linking of hydrogel networks which lead to poor swelling [45]. The nanocomposite gradually increased up to 4 h, and then water squeezed out with an increase in time. Thus, the ionic gels swelled more in water than in the saline solutions because the charge of ions present in the salt solutions had a greater influence on the swelling characteristics of the gel.

3.3. Characterization of silver nanocomposite

3.3.1. FTIR spectroscopy

FTIR transmission spectra for the prepared silver nanoparticles using plant extract, carbopol–alginate beads (CAA), and Ag-incorporated CAA beads are shown in Fig. 3. From the curve of (Fig. 3(a)), it could be seen that the characteristic peaks of silver nanoparticles, the appearance of a peak at 3,211 cm⁻¹ is assigned to O–H stretching vibration indicating the

presence of phenolic groups present in the reducing agent, C–C stretching of aromatic compounds at $1,543\text{ cm}^{-1}$, and the CHO stretching vibration of amine groups at $1,022\text{ cm}^{-1}$. Fig. 3(b) represents the FTIR spectrum of CAA beads showing O–H bonds of alginate groups which appeared at $3,349\text{ cm}^{-1}$, and C–H stretching vibrations appeared at $2,849\text{ cm}^{-1}$. The bands observed at $1,633$ and $1,315\text{ cm}^{-1}$ attributed to the asymmetric stretching vibrations of carboxylate ion and C–N groups, respectively. Fig. 3(c) represents the strong adsorption due to OH stretch ($3,700\text{ cm}^{-1}$ broadband), CH stretch ($3,349\text{ cm}^{-1}$), antisymmetric ($1,633\text{ cm}^{-1}$), and symmetric ($1,425\text{ cm}^{-1}$) COO–stretch, an antisymmetric stretch of C–O–C ($1,022$ and 1035 cm^{-1}) were all present in the spectra of CAA beads scanned. It indicates that there is no bonding interaction between silver and the alginate. This can be corroborated from the spectra, as no difference was observed between composite beads (CAA) and the composite beads incorporated with Ag (SNC) [46]. The strong COO stretching and weak symmetric stretching occurs mainly due to the metal carboxylate interactions [47]. Unlike the previous case, the AgNPs may interact with the CAA beads mainly by Van der Waals interactions, although the Ag^+ may adsorb onto the anionic bead via electrostatic attraction before bioreduction.

3.3.2. XRD study

The diffraction pattern of the SNC hydrogel nanocomposite was observed using powder X-ray diffraction (XRD) techniques as shown in Fig. 4. The

studies gave the information on the nature of the nanocomposites. The diffraction peaks appeared at 28° , 32° , 38° , 46° , 54° , 57° , and 76° were assigned to the Bragg's reflection of (1 1 1), (2 0 0), (2 1 0), (2 2 0), (3 1 1), (2 2 2), (4 2 0) planes. These diffraction peaks firmly represent a face-centered cubic structure of crystalline silver nanoparticles (from JCPDS, No. 4-0783). The XRD spectrum confirms the presence of sharper peaks of silver nanoparticles visible in the SNC and this indicated the crystalline nature of the silver nanocomposites. The average particle size is calculated from full-width half maximum of the diffraction peaks using Scherrer formula. The average crystallite size was found to be 19 nm. The obtained SNC nanocomposite beads were well matched with theoretical and experimental 2θ positions of the peaks in the diffraction pattern and d -spacing values.

3.3.3. Scanning electron microscopy with EDAX analysis

SEM and EDAX studies were utilized to examine the morphology and elemental composition of SNC nanocomposite (Fig. 5(a)). The SEM images of silver nanoparticles containing CAA based composite gels reveal that the particles in nanocomposite film were found mostly with circular morphology. The outer surface is rough. However, some agglomeration of the particles was additionally discovered (Fig. 4(c)), and the surface was fairly harsh. It is of paramount importance that the particles are non-consistently blended in a hydrogel lattice.

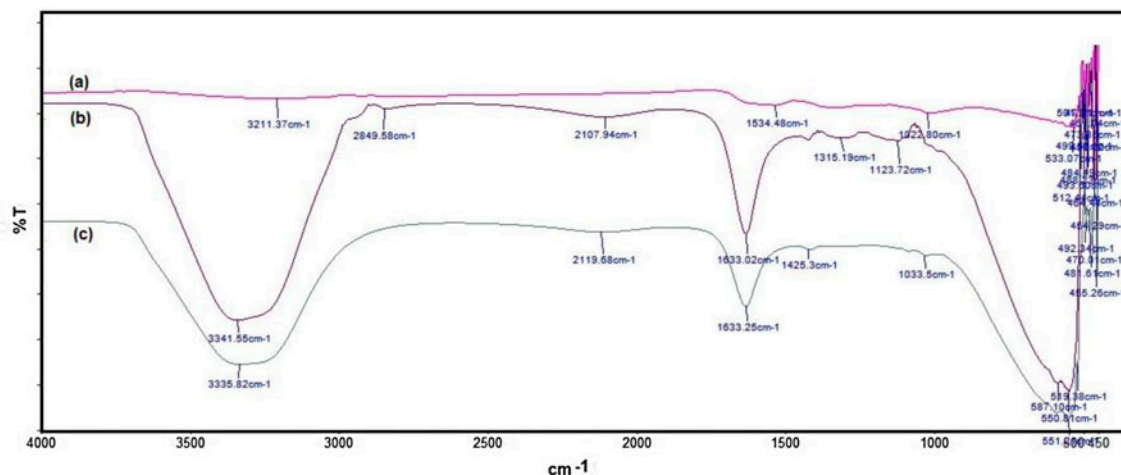


Fig. 3. (a) FTIR spectra of silver nanoparticles, (b) FTIR spectra of CAA hydrogel beads, and (c) FTIR spectra of silver-incorporated CAA hydrogel beads (SNC).

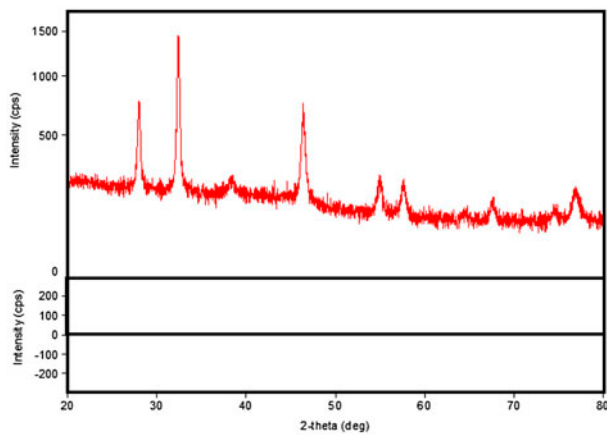


Fig. 4. XRD profile of SNC.

The detailed elemental composition of SNC nanocomposites was carried out by energy dispersive analysis of X-rays (Fig. 5(b)). It is observed that the distribution of silver nanoparticles in the CAA beads is uniform as well as homogenous. The amount of

silver and other components such as chlorine, calcium, and oxygen at the surface of the SNC nanocomposite is shown in Table 1. The peaks of copper have been detected due to the copper-coated grid of TEM. It was confirmed by EDAX that the silver ions are reduced to crystalline silver by the presence of well-resolved signals for silver. These results attributed to the formation of silver-incorporated CAA nanocomposite beads.

3.3.4. Transmission electron microscopy study

The TEM analysis of silver nanocomposite is shown in Fig. 6. TEM studies were utilized to examine the size and shape of silver nanoparticles containing CAA beads. The shape was found to be almost uniform. The average size of the particles is found to be 19.3 nm and the size of the nanoparticles varies between 11 and 20 nm. Almost 90% of the nanoparticles have a size between 11 and 16 nm, and a very small percentage of the nanoparticles have a size above the range of 16 nm.

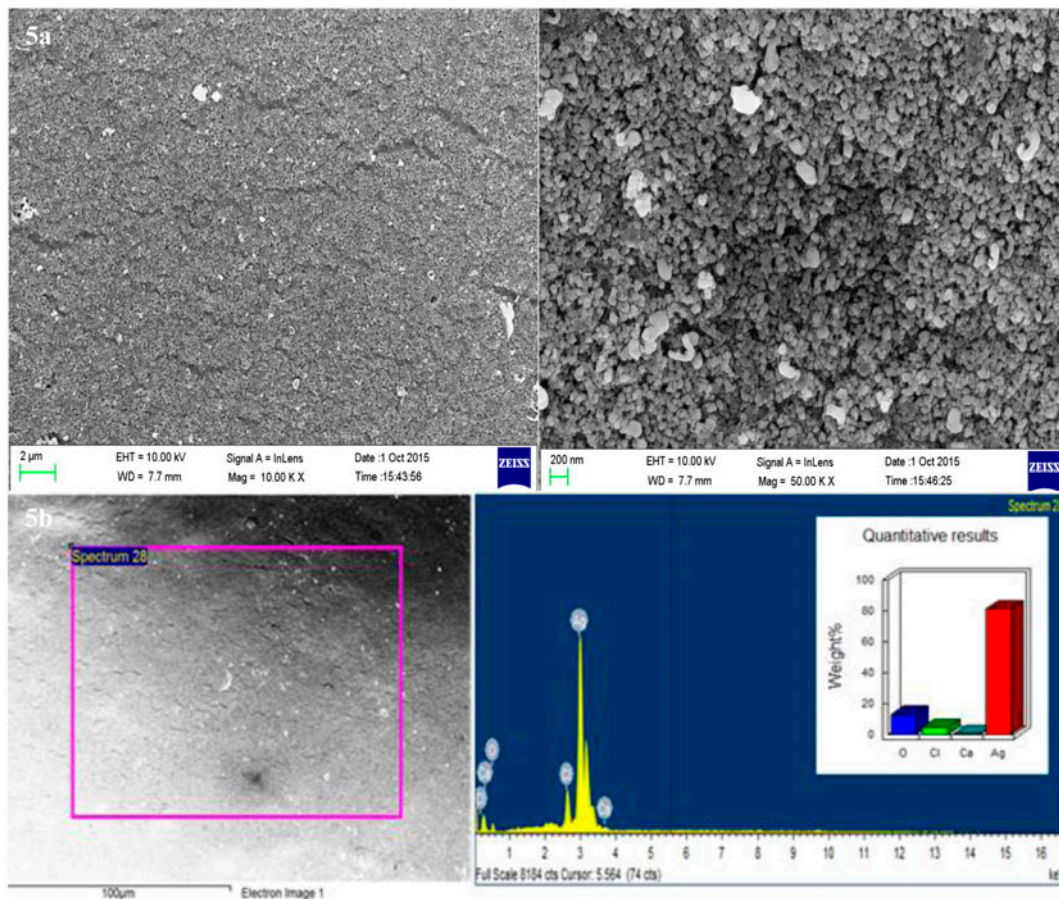


Fig. 5. (a) SEM image of SNC and (b) EDAX image of SNC.

Table 1
Elemental composition of SNC nanocomposite

Element	Weight%	Atomic%
O K	13.14	47.51
Cl K	4.85	7.92
Ca K	0.63	0.91
Ag L	81.38	43.66
Total	100	100

3.3.5. TGA and DSC study

The DTA and TGA of the starch and the gel samples are shown in Fig. 7(a) and (b), respectively. It is observed that there was two-stage decomposition and a total weight loss of 23%. The first stage of decomposition occurred at 190–200°C and was due to the evaporation of moisture content present on the surface of the silver nanocomposite. The second stage of decomposition occurred at 550–600°C. An intense exothermic peak was observed between 450–550°C which was mainly due to the crystallization of silver nanoparticles [48]. The DSC analysis also confirmed the complete decomposition of the sample.

3.4. Adsorption isotherm results

The adsorption equilibrium data were applied to the different adsorption isotherm models such as two-parameter (Langmuir and Freundlich) and three-parameter (Redlich–Peterson and Sips) adsorption

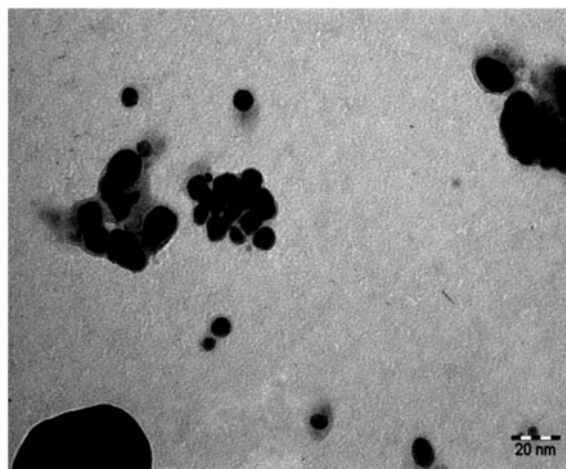


Fig. 6. TEM image of SNC.

models and the result is shown in Fig. 8. The adsorption isotherm parameters, R^2 , and error (SSE and RMSE) values were calculated and these are listed in Table 2. The higher R^2 values and the low error values were the deciding factors to provide the best-fitted adsorption isotherm model for the tested equilibrium data. The higher R^2 with lower error values were observed for Freundlich and Sips models compared to the Langmuir and Redlich–Peterson models. From Table 2, it can be seen that the value of n lies between 1 and 10. This indicates that the adsorption of MB dye onto the adsorbent is a physical process. The values of R^2 and error obtained for Freundlich model strongly

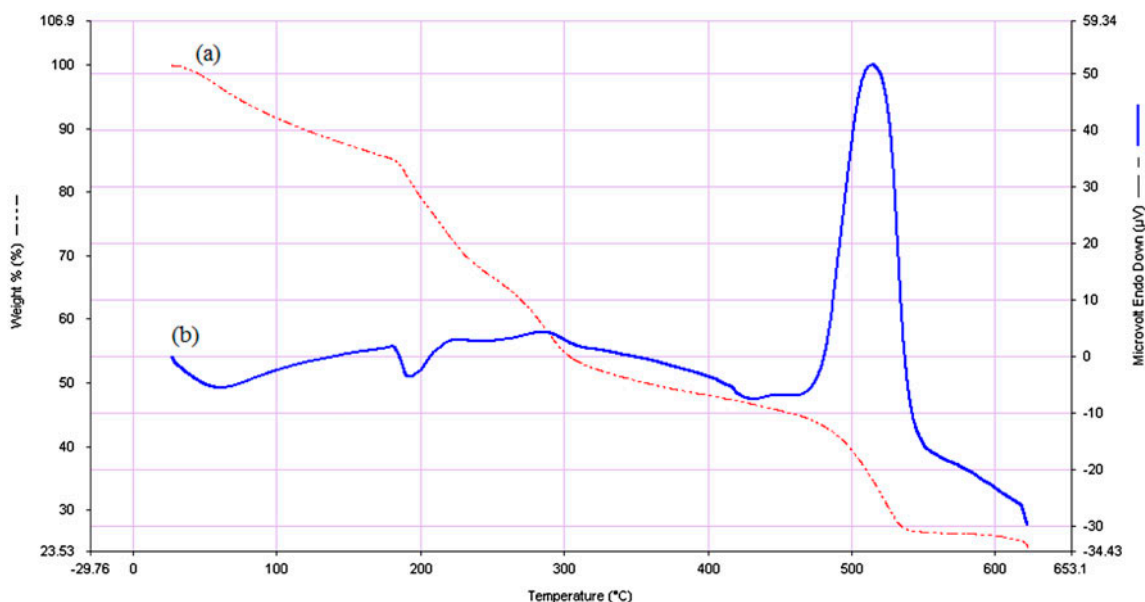


Fig. 7. (a) TGA image of SNC and (b) DSC image of SNC.

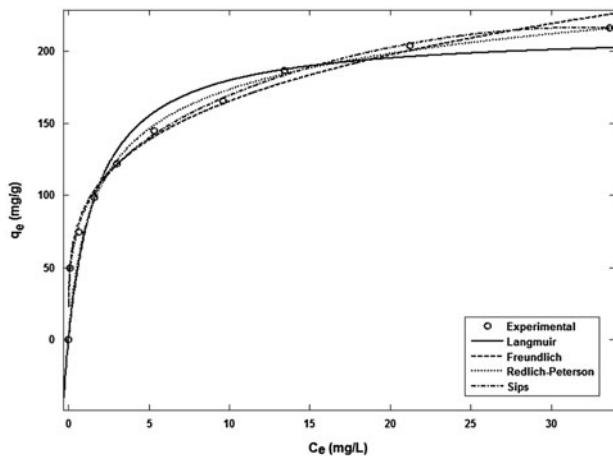


Fig. 8. Adsorption isotherm for the removal of MB dye by SNC.

indicate that the adsorption of MB dye onto the SNC follows a heterogeneous coverage on the adsorption surface. The results show that the strong chelating

Table 2
Isotherm constants for the removal of MB dye by SNC

Adsorption isotherm models	Isotherm model constants	Values
Langmuir	q_m (mg/g)	213.7
	K_L (L/mg)	0.5285
	R^2	0.9385
	SSE	2,852
	RMSE	18.88
Freundlich	K_F ((mg/g) (L/mg) ^(1/n))	91.59
	n (g/L)	3.901
	R^2	0.9939
	SSE	272.3
	RMSE	5.834
Redlich–Peterson	K_{RP} (L/g)	151.8
	a_{RP} (L/mg) ^(1/β_{RP})	1.012
	$β_{RP}$	0.8844
	R^2	0.957
	RMSE	16.61
Sips	K_S (L/g) ^{β_S}	89.26
	a_S (L/mg) ^(β_S)	3.263×10^{-7}
	$β_S$	0.2785
	R^2	0.9978
	RMSE	97.69

interaction between functional sites of MB dyes and the surface of the SNC exists. The K_F value shows that the MB dye is more efficiently removed from the wastewater by SNC. The three-parameter model provides the best fit to the adsorption equilibrium data, particularly Sips model when compared with the two-parameter models. This indicates that the adsorption of MB dye onto the SNC followed the heterogeneous adsorption process.

3.5. Adsorption kinetic results

The adsorption kinetic data was explained with the pseudo-first-order, pseudo-second-order and Elovich kinetic models to know the type of adsorption process and the results are shown in Fig. 9. The adsorption kinetic parameters, R^2 , and error (SSE and RMSE) values were calculated using MATLAB R2009 software and these are listed in Table 3. From Table 3, it is observed that higher R^2 with low error values was observed for pseudo-first-order kinetic model as against the pseudo-second-order and Elovich kinetic models. This was further confirmed by evidence from the comparison of equilibrium adsorption capacity of experimental and calculated values. Very little difference between the $q_{e,cal}$ and $q_{e,exp}$ values were observed for the pseudo-first-order kinetic model. The low R^2 , high error values, and the large difference between $q_{e,cal}$ and $q_{e,exp}$ values were observed for the pseudo-second-order kinetic model. This indicates that the adsorption of MB dye onto to SNC does not follow the pseudo-second-order kinetic model. Elovich kinetic model discusses the chemisorption on heterogeneous surfaces. This model does not provide any definite

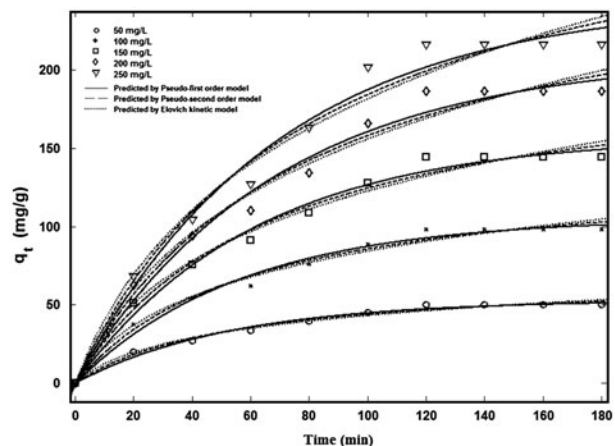


Fig. 9. Adsorption kinetics for the removal of MB dye by SNC.

Table 3
Kinetics constants for the removal of MB dye by SNC

Kinetic model	Parameters	Concentration of MB dye solution (mg/L)				
		50	100	150	200	250
Pseudo-first-order equation	k_1 (min^{-1})	0.01884	0.01769	0.01625	0.01469	0.01453
	$q_{e,\text{cal}}$ (mg/g)	52.86	105.3	157.7	208.7	244.7
	R^2	0.9886	0.9852	0.9881	0.9833	0.9833
	SSE	28.62	145.7	258.7	619.2	869.8
	RMSE	1.892	4.268	5.687	8.798	10.43
Pseudo-second-order equation	k_2 (g/mg min)	0.00027	0.00012	6.996×10^{-5}	4.43×10^{-5}	3.603×10^{-5}
	$q_{e,\text{cal}}$ (mg/g)	67.92	137	209.9	283.9	336.5
	$q_{e,\text{exp}}$ (mg/g)	50.015	98.492	145.152	187.525	217.158
	R^2	0.9886	0.9853	0.9869	0.9816	0.9788
	SSE	28.53	144.2	284.4	684.2	1,103
Elovich kinetic equation	α (mg/g min)	0.0142	0.0055	0.00265	0.00145	0.001097
	β (g/mg)	6.884	15.36	25.15	36.03	43.85
	R^2	0.9859	0.9833	0.9842	0.9791	0.974
	SSE	35.25	164.7	344.7	778	1,357
	RMSE	2.099	4.537	6.564	9.862	13.03

mechanism. Even though this model does not explain any specific mechanism, it has been applied to confirm the chemisorption mechanism. Elovich model may also use to explain the adsorption kinetic for the removal of MB dye by SNC because the adsorbent possesses the heterogeneous surface.

4. Conclusion

This paper has focused on the biosynthesis of silver nanocomposite beads (SNC) using *M. maderaspatna* plant extract. The synthesized SNC was characterized by FTIR, SEM, TEM, XRD, and TGA analyses. The characterization results showed that the SNC possess excellent adsorption properties. The results further confirmed that the biosynthesized nanocomposites are of crystalline nature and the size was controlled in the range of 19 nm. The nanocomposites exhibited excellent adsorption property toward the removal of MB dye from the aqueous solution. The adsorption equilibrium data followed the Freundlich and Sips adsorption isotherm models. The maximum monolayer adsorption capacity of the SNC for MB dye was found to be 213.7 mg/g. The adsorption kinetic data were best described by the pseudo-first-order kinetic model. Finally, it was concluded that the prepared adsorbent can be successfully applied for the removal of dye from the wastewater.

References

- [1] Y.S. Karnjkar, R.M. Dinde, N.M. Dinde, K.N. Bawankar, S.P. Hinge, A.V. Mohod, P.R. Gogate, Degradation of magenta dye using different approaches based on ultrasonic and ultraviolet irradiations: Comparison of effectiveness and effect of additives for intensification, *Ultrason. Sonochem.* 27 (2015) 117–124.
- [2] L. Das, S. Chatterjee, D.B. Naik, S. Adhikari, Role of surfactant derived intermediates in the efficacy and mechanism for radiation chemical degradation of a hydrophobic azo dye, 1-phenylazo-2-naphthol, *J. Hazard. Mater.* 298 (2015) 19–27.
- [3] M. Moussawi, A. Hijazi, H. Hamad, H. Rammal, W. Rammal, M. Alameh, D. Naoufal, Biosorption of methylene blue from waste water using *Scabiosa prolifera* (*Carmel Daisy*), *World J. Pharm. Res.* 3 (2014) 45–56.
- [4] A. Mondal, B. Adhikary, D. Mukherjee, Room-temperature synthesis of air stable cobalt nanoparticles and their use as catalyst for methyl orange dye degradation, *Colloids Surf., A* 482 (2015) 248–257.
- [5] L. Liu, J. Zhang, Y. Tan, Y. Jiang, M. Hu, S. Li, Q. Zhai, Rapid decolorization of anthraquinone and triphenylmethane dye using chloroperoxidase: Catalytic mechanism, analysis of products and degradation route, *Chem. Eng. J.* 244 (2014) 9–18.
- [6] E. Franciscon, M.J. Grossman, J.A. Paschoal, F.G. Reyes, L.R. Durrant, Decolorization and biodegradation of reactive sulfonated azo dyes by a newly isolated *Brevibacterium* sp. strain VN-15, *SpringerPlus* 1 (2012) 37.
- [7] P.S. Kumar, S. Ramalingam, C. Senthamarai, M. Niranjana, P. Vijayalakshmi, S. Sivasan, Adsorption of dye from aqueous solution by cashew nut shell: Studies on equilibrium isotherm, kinetics and thermodynamics of interactions, *Desalination* 261 (2010) 52–60.

- [8] A. Zuorro, R. Lavecchia, Evaluation of UV/H₂O₂ advanced oxidation process (AOP) for the degradation of diazo dye Reactive Green 19 in aqueous solution, *Desalin. Water Treat.* 52 (2014) 1571–1577.
- [9] K. Paździor, A. Klepacz-Smółka, S. Ledakowicz, J. Sójka-Ledakowicz, Z. Mrozińska, R. Żyła, Integration of nanofiltration and biological degradation of textile wastewater containing azo dye, *Chemosphere* 75 (2009) 250–255.
- [10] A.R. Khataee, M.N. Pons, O. Zahraa, Photocatalytic degradation of three azo dyes using immobilized TiO₂ nanoparticles on glass plates activated by UV light irradiation: Influence of dye molecular structure, *J. Hazard. Mater.* 168 (2009) 451–457.
- [11] M.T. Yagub, T.K. Sen, S. Afroze, H.M. Ang, Dye and its removal from aqueous solution by adsorption: A review, *Adv. Colloid Interface Sci.* 209 (2014) 172–184.
- [12] K.S. Bharathi, S.T. Ramesh, Removal of dyes using agricultural waste as low-cost adsorbents: A review, *Appl. Water Sci.* 3 (2013) 773–790.
- [13] A.K. Jain, V.K. Gupta, A. Bhatnagar, Utilization of industrial waste products as adsorbents for the removal of dyes, *J. Hazard. Mater.* 101 (2003) 31–42.
- [14] X. Qu, P.J.J. Alvarez, Q. Li, Applications of nanotechnology in water and wastewater treatment, *Water Res.* 47 (2013) 3931–3946.
- [15] D.K. Tiwari, J. Behari, P. Sen, Application of nanoparticles in wastewater treatment, *World Appl. Sci. J.* 3 (2008) 417–433.
- [16] B. Wen, J. Ma, C. Chen, W. Ma, H. Zhu, J. Zhao, Supported noble metal nanoparticles as photo/sono-catalysts for synthesis of chemicals and degradation of pollutants, *Sci. China Chem.* 54 (2011) 887–897.
- [17] V.K. Vidhu, D. Philip, Catalytic degradation of organic dyes using biosynthesized silver nanoparticles, *Micron* 56 (2014) 54–62.
- [18] T. Jiao, H. Guo, Q. Zhang, Q. Peng, Y. Tang, X. Yan, Reduced graphene oxide-based silver nanoparticle-containing composite hydrogel as highly efficient dye catalysts for wastewater treatment, *Nat. Publ. Gr.* 5 (2015) 1–12.
- [19] H. Ps, L. Joseph, A. Dhanya, Photocatalytic degradation of textile dyes by hydrogel supported titanium dioxide nanoparticles, *J. Environ. Eng. Ecol. Sci.* 2 (2013) 2.
- [20] M.M. Perju, E.S. Dragan, Removal of azo dyes from aqueous solutions using chitosan-based composite hydrogel, *Ion Exch. Lett.* 3 (2010) 7–11.
- [21] P. Bansal, J.S. Duhan, S.K. Gahlawat, Biogenesis of nanoparticles: A review, *Afr. J. Biotechnol.* 13 (2014) 2778–2785.
- [22] V. Patel, D. Berthold, P. Puranik, M. Gantar, Screening of cyanobacteria and microalgae for their ability to synthesize silver nanoparticles with antibacterial activity, *Biotechnol. Rep.* 5 (2015) 112–119.
- [23] S. Ahmed, M. Ahmad, B.L. Swami, S. Ikram, Green synthesis of silver nanoparticles using *Azadiracta indica* aqueous leaf extract, *J. Rad. Res. Appl. Sci.* 9 (2016) 1–7, doi: 10.1016/j.jrras.2015.06.006.
- [24] G. Vasapollo, R.D. Sole, L. Mergola, M.R. Lazzoi, A. Scardino, S. Scorrano, G. Mele, Molecularly imprinted polymers: Present and future prospective, *Int. J. Mol. Sci.* 12 (2011) 5908–5945.
- [25] G. Chitra, G. Balasubramani, R. Ramkumar, R. Sowmiya, P. Perumal, *Mukia maderaspatana* (Cucurbitaceae) extract-mediated synthesis of silver nanoparticles to control *Culex quinquefasciatus* and *Aedes aegypti* (Diptera: Culicidae), *Parasitol. Res.* 114 (2015) 1407–1415.
- [26] P. Thoniyot, M.J. Tan, A.A. Karim, D.J. Young, X.J. Loh, Nanoparticle–hydrogel composites: Concept, design, and applications of these promising, multifunctional materials, *Adv. Sci.* 2 (2015) 1–13.
- [27] S.H. Neau, M.Y. Chow, G.A. Hileman, M.J. Durrani, F. Gheyas, B.A. Evans, Formulation and process considerations for beads containing Carbopol® 974P, NF resin made by extrusion-spheronization, *Int. J. Pharm.* 199 (2000) 129–140.
- [28] G.S. Bommareddy, S. Paker-Leggs, K.K. Saripella, S.H. Neau, Extruded and spheronized beads containing Carbopol® 974P to deliver nonelectrolytes and salts of weakly basic drugs, *Int. J. Pharm.* 321 (2006) 62–71.
- [29] J.M. López-Cacho, P.L. González-R, B. Talero, A.M. Rabasco, M.L. González-Rodríguez, Robust optimization of alginate-carbopol 940 bead formulations, *Sci. World J.* 2012 (2012) 1–15.
- [30] M. Ghaffari-Moghaddam, R. Hadi-Dabanlou, Plant mediated green synthesis and antibacterial activity of silver nanoparticles using *Crataegus douglasii* fruit extract, *J. Ind. Eng. Chem.* 20 (2014) 739–744.
- [31] S. Hua, H. Ma, X. Li, H. Yang, A. Wang, pH-sensitive sodium alginate/poly(vinyl alcohol) hydrogel beads prepared by combined Ca²⁺ crosslinking and freeze-thawing cycles for controlled release of diclofenac sodium, *Int. J. Biol. Macromol.* 46 (2010) 517–523.
- [32] P.S. Kumar, S. Ramalingam, K. Sathishkumar, Removal of methylene blue dye from aqueous solution by activated carbon prepared from cashew nut shell as a new low-cost adsorbent, *Korean J. Chem. Eng.* 28 (2011) 149–155.
- [33] I.D. Mall, V.C. Srivastava, N.K. Agarwal, Removal of Orange-G and methyl violet dyes by adsorption onto bagasse fly ash—Kinetic study and equilibrium isotherm analyses, *Dyes Pigm.* 69 (2006) 210–223.
- [34] I. Langmuir, The adsorption of gases on plane surfaces of glass, mica and platinum, *J. Am. Chem. Soc.* 40 (1918) 1361–1403.
- [35] H.M.F. Freundlich, Over the adsorption in solution, *J. Phys. Chem.* 57 (1906) 385–470.
- [36] L. Jossens, J.M. Prausnitz, W. Fritz, E.U. Schlünder, A.L. Myers, Thermodynamics of multi-solute adsorption from dilute aqueous solutions, *Chem. Eng. Sci.* 33 (1978) 1097–1106.
- [37] R.J. Sips, On the structure of a catalyst surface, *Chem. Phys.* 16 (1948) 490–495.
- [38] S. Lagergren, About the theory of so-called adsorption of soluble substances, *Kungliga Svenska Vetensk. Handl.* 24 (1898) 1–39.
- [39] Y.S. Ho, G. McKay, Pseudo-second order model for sorption processes, *Process Biochem.* 34 (1999) 451–465.
- [40] S.H. Chien, W.R. Clayton, Application of Elovich equation to the kinetics of phosphate release and sorption in soils, *Soil Sci. Soc. Am. J.* 44 (1980) 265–268.
- [41] A. Roucoux, J. Schulz, H. Patin, Reduced transition metal colloids: A novel family of reusable catalysts? *Chem. Rev.* 102 (2002) 3757–3778.
- [42] Q.H. Tran, V.Q. Nguyen, A. Le, Silver nanoparticles: Synthesis, properties, toxicology, applications and

- perspectives, *Adv. Nat. Sci.: Nanosci. Nanotechnol.* 4 (2013) 033001.
- [43] M.A. Bhosale, B.M. Bhanage, Silver nanoparticles: Synthesis, characterization and their application as a sustainable catalyst for organic transformations, *Curr. Org. Chem.* 19 (2015) 708–727.
- [44] Y. Chen, H. Tan, Crosslinked carboxymethylchitosan-g-poly(acrylic acid) copolymer as a novel superabsorbent polymer, *Carbohydr. Res.* 341 (2006) 887–896.
- [45] S. Hua, A. Wang, Synthesis, characterization and swelling behaviors of sodium alginate-g-poly(acrylic acid)/sodium humate superabsorbent, *Carbohydr. Polym.* 75 (2009) 79–84.
- [46] S. Lin, R. Huang, Y. Cheng, J. Liu, B.L.T. Lau, M.R. Wiesner, Silver nanoparticle-alginate composite beads for point-of-use drinking water disinfection, *Water Res.* 47 (2013) 3959–3965.
- [47] S.K. Papageorgiou, E.P. Kouvelos, E.P. Favvas, A.A. Sapalidis, G.E. Romanos, F.K. Katsaros, Metal-carboxylate interactions in metal-alginate complexes studied with FTIR spectroscopy, *Carbohydr. Res.* 345 (2010) 469–473.
- [48] P. Laurienzo, M. Malinconico, A. Motta, A. Vicinanza, Synthesis and characterization of a novel alginate-poly(ethylene glycol) graft copolymer, *Carbohydr. Polym.* 62 (2005) 274–282.